Jinrong Li
National Key Laboratory of Science and Technology on Advanced Composites in Special Environments,
Harbin Institute of Technology,
Harbin 150080, China
e-mail: lijinrong193@163.com

Xiongfei Lv
Department of Astronautical Science and Mechanics,
Harbin Institute of Technology,
Harbin 150001, China
e-mail: lxf642491517@qq.com

Liwu Liu
Department of Astronautical Science and Mechanics,
Harbin Institute of Technology,
Harbin 150001, China
e-mail: liuliwu_006@163.com

Yanju Liu
Department of Astronautical Science and Mechanics,
Harbin Institute of Technology,
Harbin 150001, China
e-mail: yj_liu@hit.edu.cn

Jinsong Leng[1]
National Key Laboratory of Science and Technology on Advanced Composites in Special Environments,
Harbin Institute of Technology,
Harbin 150080, China
e-mail: lengjs@hit.edu.cn

Computational Model and Design of the Soft Tunable Lens Actuated by Dielectric Elastomer

Inspired by the accommodation mechanism of the human eye, several soft tunable lenses have been fabricated and demonstrated the capability of controllable focus tuning. This paper presents a computational model of a dielectric elastomer-based soft tunable lens with a compact structure that is composed of a lens frame, two soft films, and the optically transparent fluid enclosed inside. The two soft films, respectively, serve as the active film and passive film. The active film is a dielectric elastomer film and can be coated with the annular electrode or circular electrode. The deformation of the lenses with both electrode configurations can all be formulated by a boundary value problem with different boundary conditions and be solved as the initial value problem using the shooting method. Two common failure modes of loss of tension and electrical breakdown are considered in the calculation of the lens. The computational results can well fit the experimental data. The focus tuning performances as well as the distributions of stretches, stresses, and electric field in the active films of the lenses with two different electrode configurations are compared. The influences of several parameters on the performances of the lenses are discussed, such that the tunable lens can be designed to have maximum focal length change or to be optimized based on different application requirements.
[DOI: 10.1115/1.4046896]

Keywords: soft tunable lens, dielectric elastomer, computational model, lens design, structures

Introduction

The conventional focus tuning systems usually have several stacked lenses, and the focal length is tuned by adjusting the distance between the lenses. Motors or gears are used to drive such systems, making the system complex and cumbersome. The hard materials used in these systems may also restrict their biomedical applications. The observing systems in nature are evolved to fit various environments and can provide inspirations to fabricate tunable optical devices [1]. Human eye is a good reference for fabricating soft tunable lens. The mechanism for the accommodation of the human eye is illustrated in Fig. 1(*a*). The contraction of the ciliary muscle can result in the radius of curvature change on both sides of the crystalline lens and thus reduce the focal length for accommodation. Inspired by this mechanism, several soft tunable lenses have been fabricated with active polymers, such as electroactive polymers [2–5] or liquid crystal elastomers [6], and demonstrate the controllable focal length change in a compact structure.

The lenses demonstrated in Refs. [2,3] have the same geometrical structure that is illustrated in Fig. 1(*b*). The lens is composed of a lens frame, two soft films, of which one serves as the active film and the other one serves as the passive film, and the optically transparent fluid enclosed inside. The active film is a dielectric elastomer (DE) film that can reduce in thickness and expand in area when subjected to external electric field [7]. The dielectric elastomer film typically comprises a soft elastomer film and two compliant electrodes coated on both sides. In Ref. [2], circular electrodes are coated on both sides of the active film (Fig. 1(*c*)) of the lens and the electrodes must be optically transparent because the light is supposed to pass the electrode. However, the annular electrode is coated on one side of the active film (Fig. 1(*d*)) of the lens in Ref. [3] and the salty water serves as the other electrode. Since the uncoated film remains transparent, the coated electrode is not necessarily transparent and the costs can thus be reduced. For the lens with the annular electrode or circular electrode, when the active film is actuated, the lens will transform into a new configuration with changed radii of curvature of central films on both sides under the function of the inner pressure, thus varying the focal length of the lens.

This paper presents a computational model of the tunable lens with the aforementioned structure to investigate its focus tuning performance and to aid the design and optimization. The deformation of the lenses with both electrode configurations can all be formulated by a boundary value problem with different boundary conditions and be solved as the initial value problem using the shooting method. Two common failure modes of loss of tension and electrical breakdown are considered in the calculation of the lens. The computational results can well fit the experimental data.

[1]Corresponding author.

Contributed by the Applied Mechanics Division of ASME for publication in the Journal of Applied Mechanics. Manuscript received January 18, 2020; final manuscript received April 8, 2020; published online April 14, 2020. Assoc. Editor: Pedro Reis.

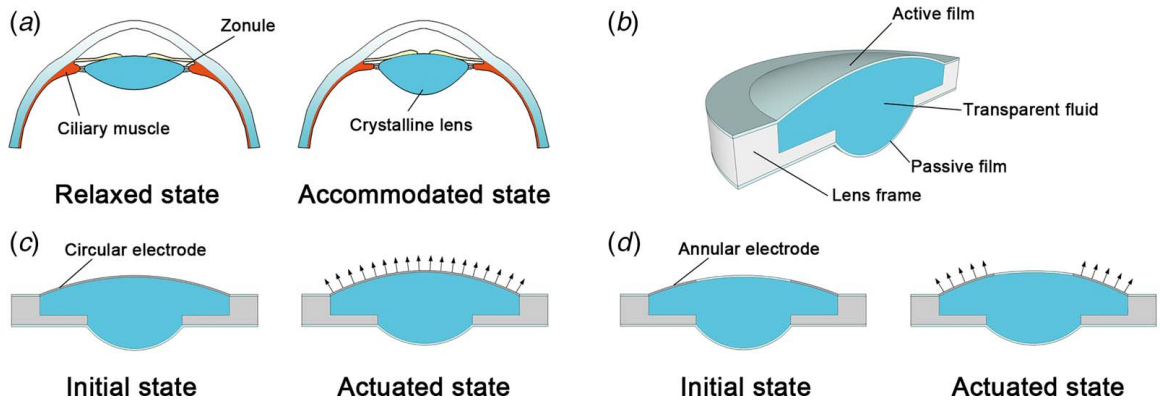

Fig. 1 (*a*) The schematic of the accommodation mechanism of the human eye. (*b*) The structure of the tunable lens discussed in this paper and the working mechanism of the lens when (c) circular electrode or (*d*) annular electrode is coated on the active film.

The focus tuning performances as well as the distributions of stretches, stresses, and electric field in the active films of the lenses with two different electrode configurations are compared. The influences of several parameters on the performances of the lenses are discussed, such that the lens can be designed to have maximum focal length change or to be optimized based on different application requirements.

Computational Model and Method

The fabrication process and basic working mechanism of the tunable lenses with both electrode configurations are similar and can be illustrated in Figs. 2(*a*)–2(*c*). First, two VHB films are adhered to both sides of the lens frame after equi-biaxial pre-stretch and, respectively, serve as the active film and passive film (Fig. 2(*a*)). The initial thickness and pre-stretch ratio of the active film are, respectively, H_a and λ_p^a, while that of the passive film are H_p and λ_p^p. The volume of the enclosed chamber is V_c. Then, the fluid with a volume of $V_0 + V_c$ is injected into the enclosed space and thus bulges both films due to the relative pressure P_0 to the atmosphere pressure (Fig. 2(*b*)). Since the amount of the fluid is small, the influence of the weight of the fluid is ignored and thus the pressure of the fluid is assumed to be uniformly distributed. When an external voltage is applied, the voltage-induced deformation of the active film will lead to the radius of curvature change in central parts of both active film and passive film, resulting in the changed focal length (Fig. 2(*c*)). In this process, the volume of the fluid remains constant and the relative internal pressure reduces to P.

After the fabrication of the lens, both the active film and passive film are in pressurized state and voltage is applied on the active film. The behavior of the circular dielectric elastomer film under external electric field and pressure has been extensively investigated in previous work [8–13]. The deformation of the film is assumed to be axisymmetric. As shown in Figs. 2(*d*)–2(*f*), in the reference state, the position of material particles can be represented by the radial coordinate X. In the pre-stretched state, the film is equi-biaxially stretched with a pre-stretch ratio λ_p. The position of material particles can be represented by the radial coordinate R and the outer radius of the film after pre-stretch is R_0. In the deformed state, the coordinate system is established at the apex of the curved film, with the z-axis along the axis of symmetry and the r-axis along

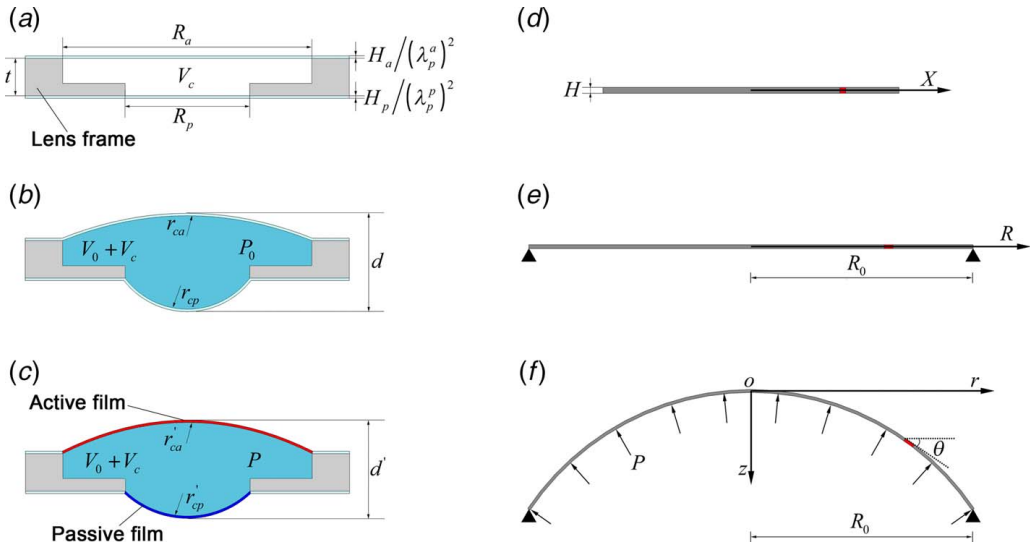

Fig. 2 The definition of some parameters when (*a*) the active and passive films are adhered to the lens frame after equi-biaxially pre-stretch, (*b*) the lens is in initial state after the transparent fluid is injected and (c) when the lens is in actuated state under external voltage. Schematic of the circular film (*d*) in reference state, (e) in pre-stretched state, and (*f*) in deformed state under the action of pressure and external voltage.

the radial direction. Considering two adjacent material particles located at X and X + dX, they take the positions at (r(X), z(X)) and (r(X + dX), z(X + dX)), respectively, after deformation. The distance of these two particles increased from dX to λ_1dX. Define θ(X) as the angle between the tangent direction and horizontal direction at point X in the deformed state. From the geometric relations, we can obtain

$$\frac{dr}{dX} = \lambda_1 \cos\,\theta \tag{1}$$

and

$$\frac{dz}{dX} = \lambda_1 \sin\,\theta \tag{2}$$

The latitudinal stretch λ_2 can be expressed as

$$\lambda_2 = \frac{r}{X} \tag{3}$$

The force balance in z-direction and latitudinal direction, respectively, gives [8,9]

$$d(\sigma_1 hr \sin\,\theta) - Prdr = 0 \tag{4}$$

and

$$d(\sigma_1 hr \cos\,\theta) + Prdz - \sigma_2 h\frac{dz}{\sin\,\theta} = 0 \tag{5}$$

where h(X) is the thickness of the deformed film. Here, we assume that the material is incompressible, namely $\lambda_1\lambda_2\lambda_3 = 1$, and thus, we can have

$$h(X) = \frac{H}{\lambda_1\lambda_2} \tag{6}$$

where H is the thickness of the film in the undeformed state. Combining Eqs. (1)–(3), and (6), we can rewrite the force balance as

$$\frac{d\theta}{dX} = -\frac{\sigma_2\lambda_1}{\sigma_1\lambda_2 X}\sin\,\theta + \frac{\lambda_1^2\lambda_2 P}{\sigma_1 H} \tag{7}$$

and

$$\frac{d\lambda_1}{dX} = \frac{1}{X\dfrac{\partial(\sigma_1/\lambda_1)}{\partial\lambda_1}}\left[\frac{\sigma_2}{\lambda_2}\cos\,\theta - \frac{\sigma_1}{\lambda_1} - \frac{\partial(\sigma_1/\lambda_1)}{\partial\lambda_2}(\lambda_1\cos\,\theta - \lambda_2)\right] \tag{8}$$

To study the electromechanically coupled deformation of the DE film, we adopt the model of ideal dielectric elastomer [14,15] that is used almost exclusively in the analyses of dielectric elastomer actuators [13,16–20]. In this model, one assumption is that the dielectric behavior of the elastomer is independent of its deformation. Under this assumption, the true electric displacement D can be written as $D = \varepsilon E$, where ε is the constant permittivity of the elastomer and E is the true electric field. Based on this model, the relations between the stresses and stretches of the DE film can be expressed as

$$\sigma_1 = \lambda_1\frac{\partial W_s(\lambda_1, \lambda_2)}{\partial\lambda_1} - \varepsilon E^2 \tag{9}$$

and

$$\sigma_2 = \lambda_2\frac{\partial W_s(\lambda_1, \lambda_2)}{\partial\lambda_2} - \varepsilon E^2 \tag{10}$$

where $W_s(\lambda_1, \lambda_2)$ is the strain energy density of the elastomer and here we employed the Gent model [21] that gives

$$W_s(\lambda_1, \lambda_2) = -\frac{\mu J_{\lim}}{2}\ln\left(1 - \frac{\lambda_1^2 + \lambda_2^2 + \lambda_1^{-2}\lambda_2^{-2} - 3}{J_{\lim}}\right) \tag{11}$$

where μ is the shear modulus of the elastomer and $J_{\lim}$ is a material constant related to the limiting stretch.

To assist the design of the tunable lens, we use the radial coordinate in the pre-stretched state for computation, which is corresponding to the state of lens before injecting fluid in Fig. 2(*a*). Some dimensionless quantities are used: $\bar{R} = R/R_0$, $\bar{r} = r/R_0$, $\bar{z} = z/R_0$, $\bar{\sigma}_1 = \sigma_1/\mu\lambda_1$, $\bar{\sigma}_2 = \sigma_2/\mu\lambda_2$, $\bar{P} = PR_0/\mu H$, and $\bar{E} = E/\sqrt{\mu/\varepsilon}$, where R_0 is the radius of the film after pre-stretch. Then, we can rewrite Eqs. (1), (2), (7), and (8) as

$$\frac{d\bar{r}}{d\bar{R}} = \frac{\lambda_1\cos\,\theta}{\lambda_p} \tag{12}$$

$$\frac{d\bar{z}}{d\bar{R}} = \frac{\lambda_1\sin\,\theta}{\lambda_p} \tag{13}$$

$$\frac{d\theta}{d\bar{R}} = -\frac{\bar{\sigma}_2}{\bar{\sigma}_1\bar{R}}\sin\,\theta + \frac{\lambda_1\lambda_2\bar{P}}{\bar{\sigma}_1\lambda_p} \tag{14}$$

$$\frac{d\lambda_1}{d\bar{R}} = \frac{1}{\bar{R}\dfrac{\partial\bar{\sigma}_1}{\partial\lambda_1}}\left[\bar{\sigma}_2\cos\,\theta - \bar{\sigma}_1 - \frac{\partial\bar{\sigma}_1}{\partial\lambda_2}(\lambda_1\cos\,\theta - \lambda_2)\right] \tag{15}$$

and the latitudinal stretch λ_2 becomes

$$\lambda_2 = \frac{\bar{r}}{\bar{R}}\lambda_p \tag{16}$$

Since the origin of the coordinate is set at the apex of the curved film and the deformation of the film is assumed to be axisymmetric, we can get the following initial values

$$\bar{r}(0) = 0,\ \ \bar{z}(0) = 0,\ \ \theta(0) = 0 \tag{17}$$

At the outer boundary ($\bar{R} = 1$), the film has adhered to the frame and thus we have

$$\bar{r}(1) = 1 \tag{18}$$

By solving the set of first-order differential equations (12)–(15) with boundary conditions (17) and (18), the inhomogeneous deformation of the curved film under given loading conditions can be obtained from the solutions $\bar{r}(\bar{R})$, $\bar{z}(\bar{R})$, $\theta(\bar{R})$, and $\lambda_1(\bar{R})$.

When calculating the deformation of the lens, the shooting method is used to numerically solve the differential equations. The active and passive films are considered separately, and the dimensionless quantities are calculated using their own geometric parameters that are illustrated in Fig. 2(*a*). For the passive film, there is no electrical load, indicating $E = 0$ in Eqs. (9) and (10). For the active film with the circular electrode, the electric field along the thickness of the film under the external voltage Φ can be expressed as

$$E = \Phi\lambda_1\lambda_2/H \tag{19}$$

When calculating the deformation of the passive film or the active film with the circular electrode, the initial values of $\bar{r}(0) = 0, \bar{z}(0) = 0,\ \theta(0) = 0$ and $\lambda_1(0) = \lambda_1'$ are given to obtain a set of solutions, of which λ_1' is the guessed value of the longitudinal stretch at the apex and λ_1' is varied until boundary condition (18) is satisfied.

When calculating the deformation of the active film with the annular electrode, voltage is only applied to the coated area, namely

$$E = \begin{cases} 0, & 0 \le \bar{R} < \bar{R}_e \\ \Phi\lambda_1\lambda_2/H, & \bar{R}_e \le \bar{R} \le 1 \end{cases} \tag{20}$$

where $\bar{R}_e = R_e/R_a$ is the dimensionless inner radius of the annular electrode. At the inner edge of the electrode, the continuity conditions should be given considering that both the deformation and longitudinal stress are continuous, namely,

$$\bar{r}(\bar{R}_{e-}) = \bar{r}(\bar{R}_{e+}),\ \ \bar{z}(\bar{R}_{e-}) = \bar{z}(\bar{R}_{e+}),\ \ \theta(\bar{R}_{e-}) = \theta(\bar{R}_{e+}),$$
$$\bar{\sigma}_1(\bar{R}_{e-}) = \bar{\sigma}_1(\bar{R}_{e+}) \tag{21}$$

In numerical computation, the initial values $\bar{r}(0)=0,\ \bar{z}(0)=0,\theta(0)=0$, and $\lambda_1(0)=\lambda_1'$ are first given to solve the differential equations in the interval $[0, \bar{R}_e]$. Then we find the value of λ_1^* so that

$$\bar{\sigma}_1(\lambda_1^*, \lambda_2(\bar{R}_e))|_{E=E(\lambda_1^*,\lambda_2(\bar{R}_e))} = \bar{\sigma}_1(\lambda_1(\bar{R}_{e-}), \lambda_2(\bar{R}_e))|_{E=0} \tag{22}$$

Then, $\bar{r}(\bar{R}_e)$, $\bar{z}(\bar{R}_e)$, $\theta(\bar{R}_e)$, and λ_1^* are used as the initial values to solve the differential equations (12)–(15) in the interval $[\bar{R}_e, 1]$. Similarly, λ_1' is varied until the boundary condition (18) is satisfied.

When fabricating the DE tunable lens, the amount of the injected fluid can be accurately controlled and remains constant during the deformation. So, the fluid volume V_0+V_c is regarded as a parameter of the tunable lens, and the dimensionless quantities $\bar{V}_0=V_0/\pi R_a^2 t$ and $\bar{V}_c=V_c/\pi R_a^2 t$ are utilized. For a lens with a given $\bar{V}_0$, the inner pressure P is to be determined to obtain its configuration under the external voltage Φ. A value of the internal pressure P' is first guessed to get the solutions $(\bar{r}_a,\ \bar{z}_a)$ and $(\bar{r}_p,\ \bar{z}_p)$ using the aforementioned method, which, respectively, give the deformation of the active film and passive film. After getting the deformation of the passive film, the dimensionless results of $\bar{r}_p$ and $\bar{z}_p$ are further scaled by a coefficient $\alpha=R_p/R_a$, which is the ratio of the radius of passive film to the radius of the active film. The sum of the dimensionless bulging volumes of both films can be calculated as

$$\bar{V}=\frac{1}{\bar{t}}\int_0^1 \bar{r}_a^2\frac{d\bar{z}_a}{d\bar{R}_a}d\bar{R}_a+\frac{\alpha^3}{\bar{t}}\int_0^1 \bar{r}_p^2\frac{d\bar{z}_p}{d\bar{R}_p}d\bar{R}_p \tag{23}$$

where $\bar{t}=t/R_a$. The value of P' is tuned until $\bar{V}=\bar{V}_0$. In all the numerical computation processes, the guessed values are not varied until the relative tolerance is within $\pm 0.01\%$.

After the configuration of the lens is determined, we can calculate the focal length of the lens using the thick lens formula

$$\frac{1}{f}=(n-1)\left[\frac{1}{r_{ca}}+\frac{1}{r_{cp}}-\frac{(n-1)d}{nr_{ca}r_{cp}}\right] \tag{24}$$

where n is the refractive index of the fluid and r_{ca} and r_{cp} are, respectively, the radii of curvature of the active film and passive film in the central area. Here, r_{ca} and r_{cp} are both positive and the signs of the radii of curvature in Eq. (24) are already considered regarding a double convex lens. Dimensionless quantities $\bar{f}=f/R_a$, $\bar{r}_{ca}=r_{ca}/R_a$, $\bar{r}_{cp}=r_{cp}/R_a$, and $\bar{d}=d/R_a$ are used in the calculation.

Results and Discussions

To calculate the performance of the lens with the annular electrode, we use the parameters that are listed in Table 1, which are the same as the parameters of the lens demonstrated in Ref. [3], except for $\bar{V}_0(\bar{V}_0=0.509)$ which is determined so that the initial focal length of the lens is 17 mm. We also calculate the performance of the lens with circular electrode using exactly the same parameters. Figure 3(*a*) illustrates the configuration changes of the lens with annular electrode (represented by Lens-A) and the lens with circular electrode (represented by Lens-C) under the applied voltage of 5.5 kV, compared to the initial configuration. In each configuration, two sets of colors are used to differentiate the deformation of active part and passive part. The cross sections of the central parts of the deformed films can be well fitted by circular arcs, which are illustrated with the thin black solid lines in Fig. 3(*a*). So, the lens is spherical lens in both initial state and actuated state, and it is reasonable to calculate its focal length using the thick lens formula (24) with fitted radii of curvature. For Lens-A, the coated area bulges out, leading to the increase of the radii of curvature in the central areas of both the active film and passive film (Fig. 3(*b*)). Thus, the focal length of the lens increases with the rise of the applied voltage (Fig. 3(*c*)). The computational results can agree well with the experimental data using fitted shear modulus $\mu=14.6$ kPa. The failure modes of loss of tension and electrical breakdown are also considered. The loss of tension occurs when the longitudinal or latitudinal stress is negative. Wrinkles will form due to loss of tension and the configuration of the lens cannot be predicted using our model. When the electric field on the film is beyond the critical value E_c, which is set to be $50V/\mu$m [18] in this paper, electrical breakdown will occur and result in irreversible failure of the lens. The voltages corresponding to these two failure modes are marked in Fig. 3(*c*).

Table 1 Material constants and design parameters used in the calculation of the soft tunable lens

	Symbol	Value
Material constants		
Shear modulus of the dielectric elastomer (fitted value)	μ	14.6 kPa
Material constant related to the limiting stretch	$J_{\lim}$	270
Permittivity of the dielectric elastomer	ε	$4.7\varepsilon_0$
Refractive index of the transparent fluid	n	1.34 (salty water)
Design parameters		
Radius of the active film	R_a	10 mm
Radius of the passive film	R_p	5 mm
Ratio of radius of the passive film to radius of the active film	α	0.5
Pre-stretch ratio of the active film	λ_p^a	2.5
Pre-stretch ratio of the passive film	λ_p^p	1
Thickness of the active film	H_a	1 mm (VHB4910)
Thickness of the passive film	H_p	0.5 mm (VHB4905)
Volume of the enclosed fluid	$\bar{V}_0+\bar{V}_c$	$0.5+\bar{V}_c$
Inner radius of the annular electrode	$\bar{R}_e$	0.5
Depth of the lens frame	t	3 mm

For the Lens-C, both the active film and the passive film will move to the same direction, resulting in the decrease of the radius of curvature of the active film and increase of the radius of curvature of the passive film (Fig. 3(*b*)). From Eq. (24), the influence of the radius of curvature change of the passive film on the focal length is partially counteracted by the radius of curvature change of the active film. Therefore, as shown in Fig. 3(*c*), the focal length change of the Lens-C is lower than that of Lens-A under the same external voltage, especially when the voltage is high. Besides, for Lens-C, the focal length reduces slightly when the voltage is above 5600 V, due to the sharp decrease of the radius of curvature of the active film (Fig. 3(*b*)). Generally, such a decrease in focal length is not useful in practical application since the same focal length change can be realized at a relatively low voltage. It should be noted that effective numerical solution of the Lens-C cannot be obtained when the applied voltage is higher than 5750 V using our computational model and the lens does not fail under this voltage.

With the increase of the applied voltage, the pressure of the fluid inside the lens decreased smoothly (Fig. 3(*d*)). Since the deformed area of Lens-C is larger than that of Lens-A, the inner pressure of Lens-C reduces faster with the increase of the applied voltage. In the actuated state, the thickness of the lens also reduces as shown in Fig. 3(*e*), which has a reverse effect on the increase of the focal length according to Eq. (24). For Lens-C, the aperture can be regarded as the smaller diameter of the lens frame and remains constant when the voltage is applied. For Lens-A, the inner radius of the annular electrode will decrease under external voltage (Fig. 3(*a*)) and the aperture reduces accordingly (Fig. 3(*e*)). Even when the transparent electrode is used, the decrease of aperture should also be considered since the deformed area is not spherical. The aperture of Lens-A reduces by about 18.4% under the voltage corresponding to a loss of tension.

Figures 4(*a*)–4(*e*) illustrate the distributions of stretches, stresses, and electric field in the active film of the lens along the radial direction under various external voltages. The stretches and stresses of the active film of Len-C vary more smoothly than that of

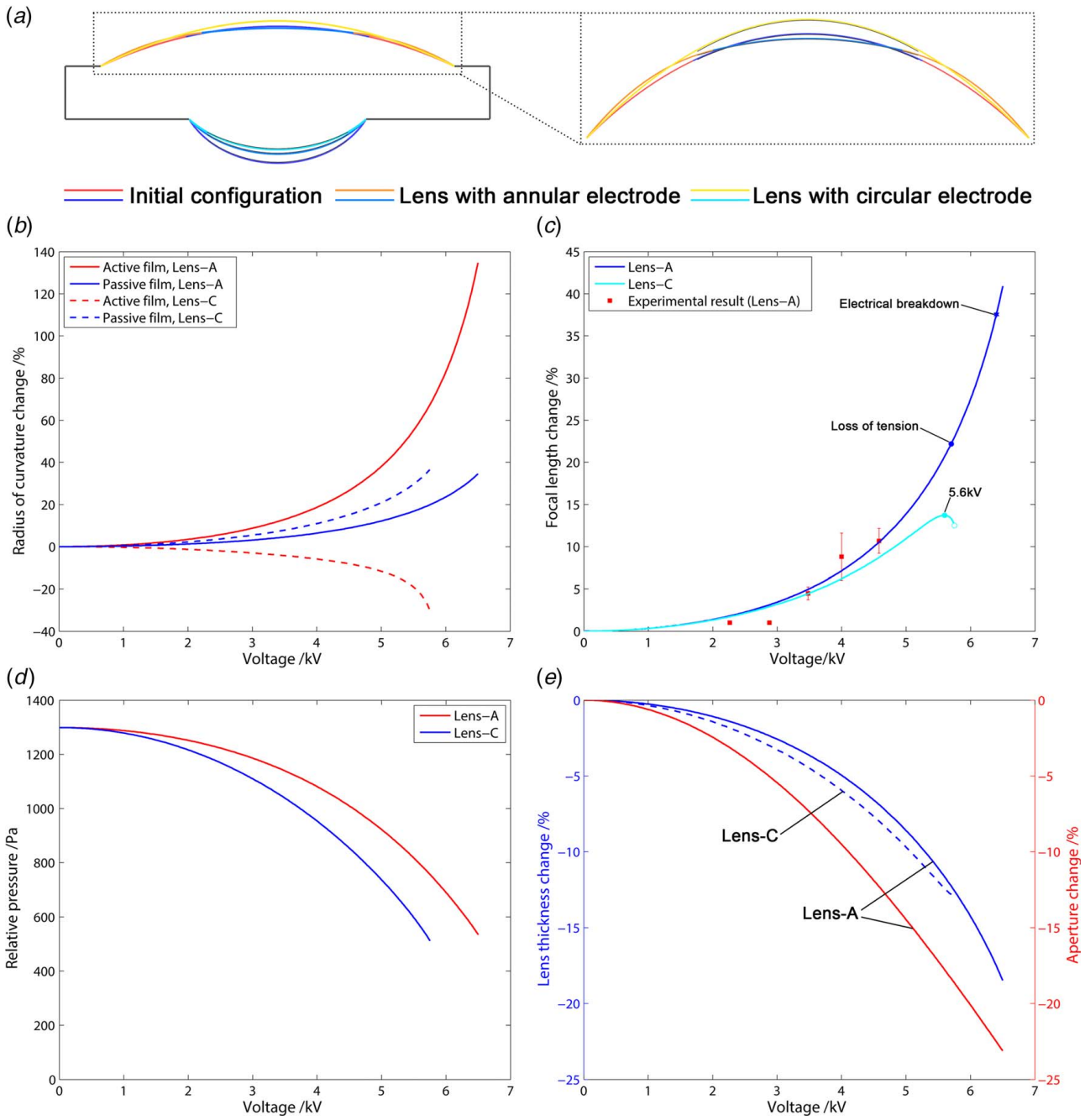

Fig. 3 (*a*) Configuration change of the lens with annular electrode and circular electrode under the applied voltage of 5.5 kV, compared to the initial configuration. The thin black lines represent the fitted circular arcs corresponding to the central parts of the deformed films. Comparison of the (*b*) radius of curvature change of the films, (*c*) focal length change, (*d*) relative pressure change, and (*e*) change in the thickness and aperture between the tunable lens with annular electrode and the tunable lens with circular electrode.

Len-A. For Len-C, the apex of the active film is in an equally bi-axial stretched state and has the maximum longitudinal and latitudinal stretch. Thus, the electrical breakdown will first occur at the apex point, of which the electric field is maximal. The point with minimum stress locates at the out boundary of the film when the voltage is low and then shifts to the apex as the increase of the voltage.

For Lens-A, all the particles in the central uncoated part of the active film have nearly the same longitudinal and latitudinal stretch ratio. That means that the central part is very close to a spherical configuration. At the inner edge of the electrode, the latitudinal stretch λ_2 and longitudinal stress $\bar{\sigma}_1$ are continuous as described in the computational model. The longitudinal stretch λ_1 has a sudden rise at the edge of the electrode while the latitudinal stress $\bar{\sigma}_2$ has a sudden drop. The edge of the electrode has the minimum latitudinal stress and thus loss of tension is prone to occur around the edge of the electrode. The edge of the electrode also has the maximum electric field at low voltage and the point near the electrode edge has the maximum electric field at relatively high voltage, which means that the electrical breakdown will occur near the edge of the electrode.

Figure 4(*e*) compared the minimum latitudinal stress $\bar{\sigma}_{2\min}$ and the maximum electric field $\bar{E}_{\max}$ of the active film in Lens-A and Lens-C. When the voltage is low, these two quantities of the

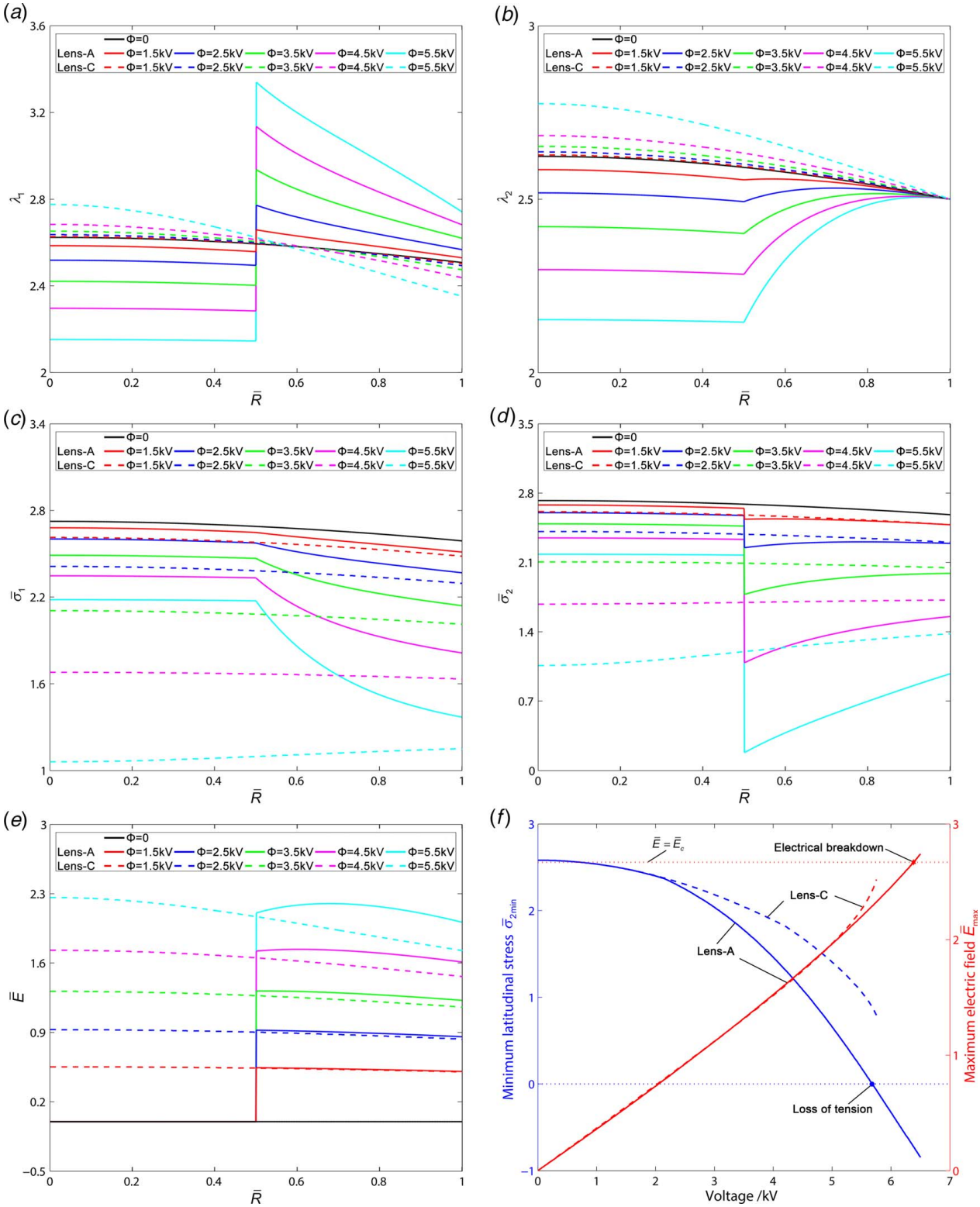

Fig. 4 The distribution of the (*a*) longitudinal stretch, (*b*) latitudinal stretch, (*c*) longitudinal stress, (*d*) latitudinal stress, and (*e*) electric field in the active film along the radial direction of tunable lens with annular and circular electrode under various external voltages. (*f*) The change of the minimum latitudinal stress and maximum electric field of the active film of the tunable lens with different electrode configurations with the increasing of the external voltage.

lenses with bot electrode configurations are very close. With the increase of the external voltage, $\bar{E}_{\max}$ of the Lens-C increases more rapidly and $\bar{\sigma}_{2\min}$ of the Lens-A decreases more rapidly. As a result, the electrical breakdown is the prior failure mode for Lens-C and loss of tension is the prior failure mode for Lens-A.

Then, we can investigate the influences of different parameters on the focus tuning performances of the tunable lenses. It should be noted that, when discussing the influence of one parameter, other parameters of the lens are fixed at the values listed in Table 1. The pre-stretch ratios of both the active film (λ_p^a) and passive film

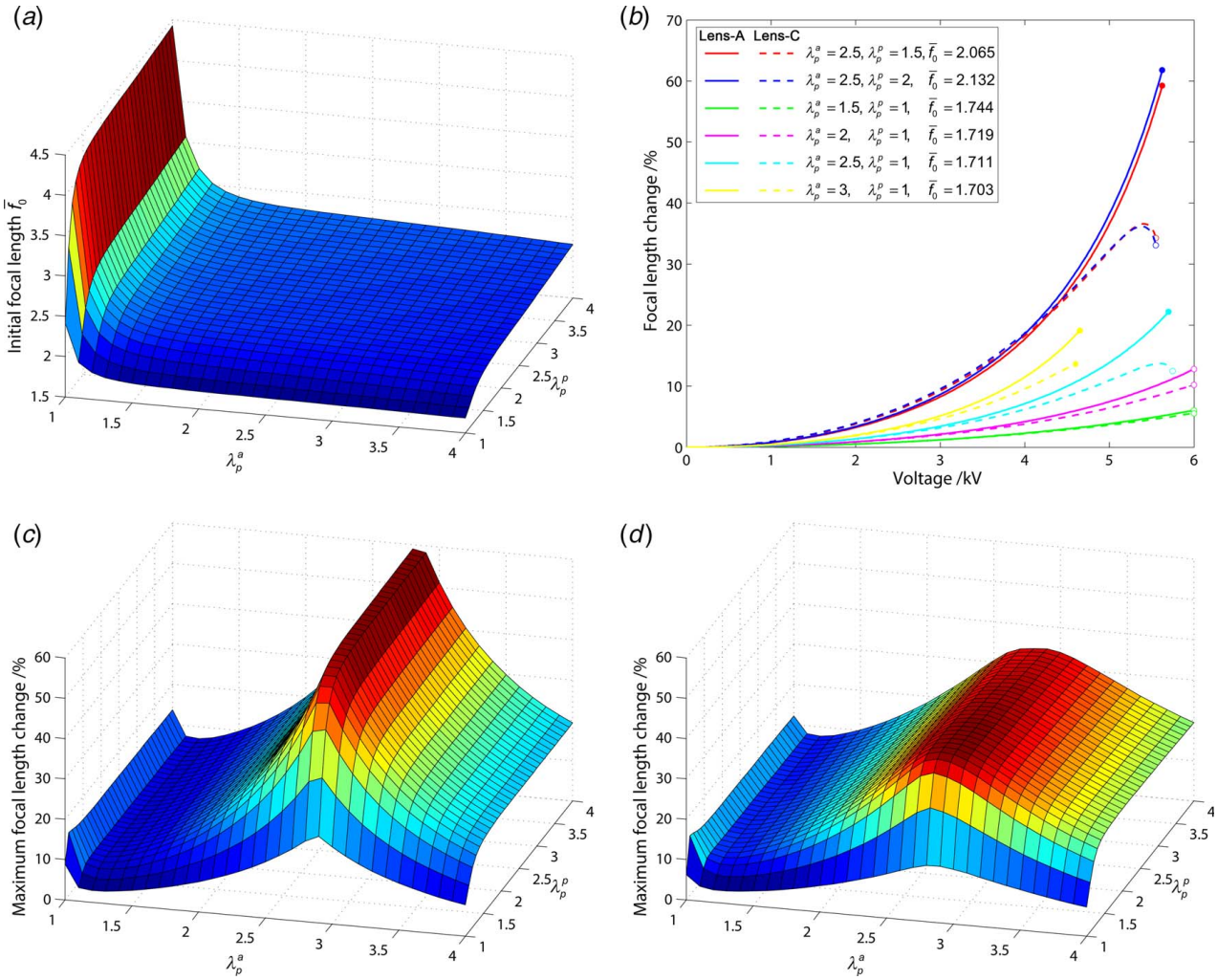

Fig. 5 (*a*) The initial focal length of the lens with various λ_p^a and λ_p^p. (*b*) Focus tuning performances of the tunable lenses with different combinations of λ_p^a and λ_p^p. Circular dot represents that the lens fails due to loss of tension and hexagram represents that the lens fails due to electrical breakdown. The point marked by a hollow circle means that the applied voltage reaches at 6 kV or effective solution cannot be obtained for Lens-C. Maximum focal length change of the tunable lens with (c) annular electrode and (*d*) circular electrode with various λ_p^a and λ_p^p.

(λ_p^p) can determine the initial focal length and focal length change of the lens. Figure 5(*a*) demonstrates the initial focal length of the lens with various λ_p^a and λ_p^p. The initial focal length has a steep drop when λ_p^a rises from 1 to 1.3. The reason is that the passive film is relatively flat and has a large radius of curvature when λ_p^a is small. The initial focal length also has a slight increase when λ_p^p increases. The change of the initial focal length is limited when both λ_p^a and λ_p^p are higher than 1.5.

Figure 5(*b*) plots the focal length change-voltage curves of the tunable lenses with different combinations of λ_p^a and λ_p^p. The solid lines represent the performances of Lenses-C and the dashed lines represent the performances of Lenses-A. The curves ended at the failure voltage, which is the minimum voltage between the voltage corresponding to loss of tension (marked by a circular dot) and the voltage corresponding to electrical breakdown (marked by a hexagram). The point marked by a hollow circle means that the applied voltage reaches at 6 kV or effective solution cannot be obtained for Lens-C. As can be seen from Fig. 5(*b*), when the voltage is low, the focal length changes of Lens-A and Lens-C are close and Lens-A will have larger focal length change at higher voltage. When λ_p^p changes from 1 to 1.5, the maximum relative focal length change of the lens can increase significantly, as a result of the larger radius of curvature change of the films on both sides. However, such change becomes little when λ_p^p changes from 1.5 to 2. The rise of λ_p^a will increase the focal length but also reduce the failure voltage, resulting in an optimal interval of λ_p^a. Figures 5(*c*) and 5(*d*), respectively, illustrate the maximum focal length change at 0–5 kV of Lens-A and Lens-C with different pre-stretch ratios. If the failure voltage is lower than 5 kV, the focal length change at failure voltage is plotted instead. When λ_p^a is between 2 and 3.5, the maximum focal length change of Len-A is obviously larger than that of Lens-C, while they are close when λ_p^a takes other values. The influences of the change of λ_p^a and λ_p^p on the performances of the lenses with both electrode configurations are similar. From these two figures, we can find that the optimal interval of λ_p^a for the lenses with both electrode configurations is 2.5–3, where larger focal length change can be achieved. The critical λ_p^a corresponding to a failure voltage of 5 kV is between 2.8 and 2.9, above which the failure voltage is smaller than 5 kV and thus the maximum focal length change is reduced. The maximum focal length change increases significantly when λ_p^p increases from 1 to 1.5. When λ_p^p is higher than 1.5, the maximum focal length change tends to be stable.

The influence of the inner radius $\bar{R}_e$ of the annular electrode is presented in Fig. 6(*a*). The actuated area decreases as $\bar{R}_e$ increases, thus generating smaller contraction of the uncoated area and leading to lower focal length change. When $\bar{R}_e = 0.7$, the focal length

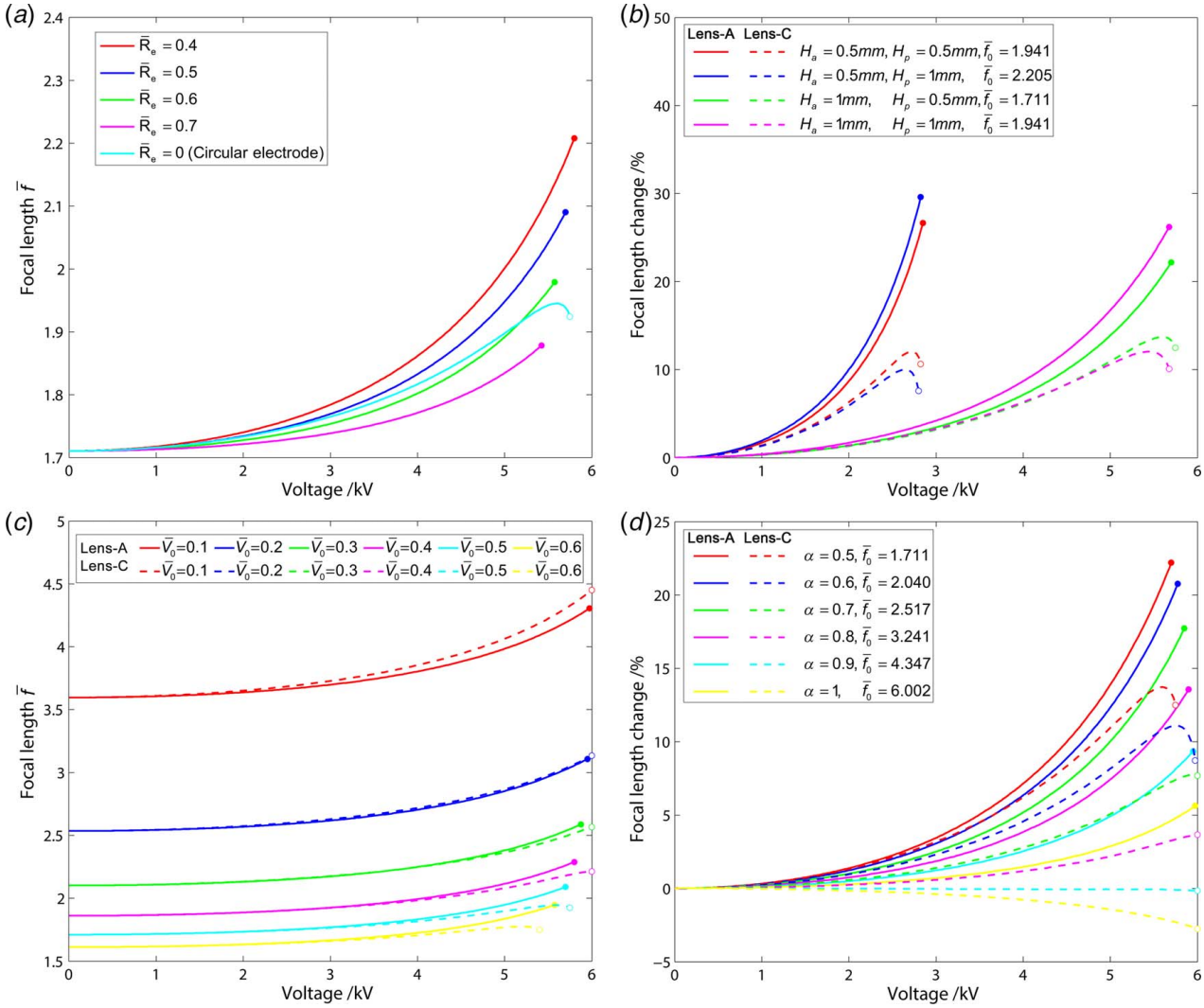

Fig. 6 The focus tuning performances of the tunable lenses with different (*a*) inner radii of annular electrode, (*b*) film thicknesses, (c) fluid volumes, and (*d*) ratios of radius of passive film to radius of active film. Circular dot represents that the lens fails due to loss of tension and the point marked by a hollow circle means that the applied voltage reaches at 6 kV or effective solution cannot be obtained for Lens-C.

change of Lens-A is already lower than that of Lens-C. The increase of $\bar{R}_e$ also slightly lowers the failure voltage. Moreover, the aperture of the lens is determined by $\bar{R}_e$ as mentioned above. Therefore, although smaller $\bar{R}_e$ can generate larger focal length change, the inner radius of the annular electrode should be chosen considering the aperture of the lens.

The thickness of the films can be easily altered by using different commercial VHB products in the fabrication of the lens. The performances of the lenses with different film thicknesses are demonstrated in Fig. 6(*b*). The lens with thinner active film can generate larger focal length change at a relatively lower voltage and has lower failure voltage. A thicker passive film raises the focal length change and has almost no influence on the failure voltage of the lens.

The volume of the enclosed fluid determines the initial configuration of the lens. As shown in Fig. 6(*c*), when $\bar{V}_0$ is small, the radii of curvature of both films are large, leading to a large initial focal length. When $\bar{V}_0 = 0.1$, the passive film of Lens-C can be flatter in the actuated state than that of Len-A. As a result, the focal length change of Lens-C is larger than that of Len-A when the amount of fluid is small. As the fluid volume increases, the initial focal length decreases and the focal length change of Lens-A gradually becomes larger than that of Lens-C. The failure voltage also reduces slightly since the films are further stretched by the increased fluid volume.

As the ratio α of the radius of passive film (R_p) to the radius of the active film (R_a) increases, the area of the passive film increases, resulting in a larger initial focal length under the constant fluid volume. The relative focal length change of the tunable lens will decrease with the increase of α. For Lens-C, since the influence of the radius of curvature change of the film on one side can be compensated by that of the film on the other side, the relative focal length change can be very small ($\alpha = 0.9$) or even negative ($\alpha = 1$) when α is high. The focal length change can decrease further when $\alpha > 1$, which is equivalent to the situation that the film with a smaller radius is actuated. Therefore, if circular transparent electrodes are coated on both films of the lens, it is possible to expand the focal length change range through choosing which film is active, depending on different application requirements. For example, for a lens with the same geometric parameters as listed in Table 1, when the pre-stretch ratio of the film with larger radius is 2.5 and the ratio of the film with smaller radius is 1.5, the achievable relative focal length change can be from −27.9% to 36.6%, as shown in Fig. 7.

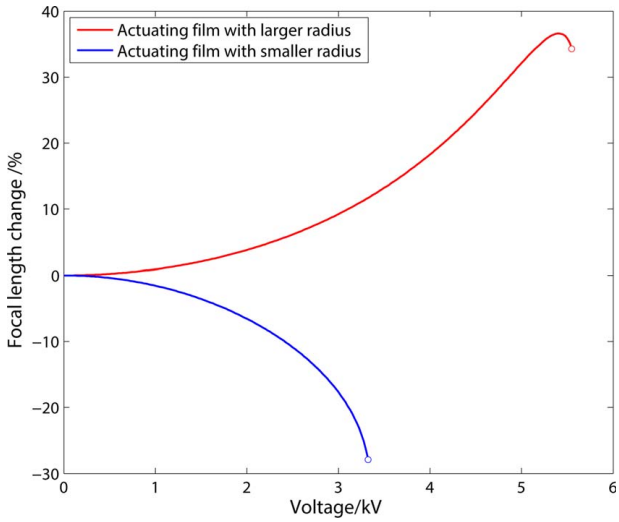

Fig. 7 Focus tuning performance of the tunable lens, of which circular transparent electrodes are coated on both films, when different films are actuated. The point marked by a hollow circle means that the effective solution cannot be obtained.

Conclusions

In this paper, a computational model is presented for the dielectric elastomer tunable lens with a compact structure as demonstrated in Refs. [2,3]. The calculation results can well fit the experimental results in Ref. [3] with a fitted shear modulus. The adjusting of the focus of the lens is realized through the radius of curvature change on both sides of the lens due to electrically induced deformation of the dielectric elastomer. When an external voltage is applied, the radii of curvature of the films on both sides of the lens with the annular electrode increase, increasing the focal length. For the lens with the circular electrode, the film on one side has an increased radius of curvature while the film on the other side has a decreased radius of curvature. The influences of the radius of curvature changes on two sides can be compensated by each other. Therefore, a lens with the annular electrode is more efficient in increasing the focal length than a lens with the circular electrode and can generally obtain larger focal length change, especially at a higher voltage. However, larger focal length change can be obtained in the lens with the circular electrode if the passive film is relatively flat. Furthermore, the focal length of the lens with the circular electrode can increase or decrease depending on the parameters, while the lens with the annular electrode can only has an increasing focal length.

The influences of different parameters on the performances of the tunable lenses are also investigated. The increase of the pre-stretch ratio of the active film can increase the maximum focal length change of the tunable lens but an optimal interval exists when failure is considered. The maximum focal length change also rises with the increase of the pre-stretch ratio of the passive film and becomes stable beyond a critical value. The aperture of the lens is determined by the minor radius of the lens frame and is further restrained by the inner radius of the electrode for the lens with an annular electrode. The lens with the annular electrode can have a relatively large focal length change when the inner radius of the electrode is small. But a suitable value of electrode radius is supposed to be chosen considering the aperture. The focal length change of the lens with the circular electrode highly relies on the difference between the radii of cavities on both sides of the lens frame, as also mentioned in Ref. [2]. Actuating different films, positive and negative focal length change can be realized in one tunable lens, of which both films are coated with circular transparent electrodes. The depth of the lens frame determines the thickness of the lens and thus the initial focal length. This is not discussed in detail in this paper. In practice, the frame depth should be minimized to reduce the effect of gravity of the fluid. These results will be helpful to assist the design and optimization of the tunable lens.

Funding Data

- National Natural Science Foundation of China (Grant No. 11772109; Funder ID: 10.13039/501100001809).

References

[1] Lee, L. P., and Szema, R., 2005, "Inspirations From Biological Optics for Advanced Photonic Systems," Science, **310**(5751), pp. 1148–1150.
[2] Shian, S., Diebold, R. M., and Clarke, D. R., 2013, "Tunable Lenses Using Transparent Dielectric Elastomer Actuators," Opt. Express, **21**(7), p. 8669.
[3] Li, J., Wang, Y., Liu, L., Xu, S., Liu, Y., Leng, J., and Cai, S., 2019, "A Biomimetic Soft Lens Controlled by Electrooculographic Signal," Adv. Funct. Mater., **29**(36), p. 1903762.
[4] Carpi, F., Frediani, G., Turco, S., and De Rossi, D., 2011, "Bioinspired Tunable Lens With Muscle-Like Electroactive Elastomers," Adv. Funct. Mater., **21**(21), pp. 4152–4158.
[5] Choi, D., Jeong, J., Shin, E., and Kim, S., 2017, "Focus-tunable Double Convex Lens Based on Non-Ionic Electroactive gel," Opt. Express, **25**(17), p. 20133.
[6] Petsch, S., Schuhladen, S., Dreesen, L., and Zappe, H., 2016, "The Engineered Eyeball, a Tunable Imaging System Using Soft-Matter Micro-Optics," Light: Sci. Appl., **5**(7), p. e16068.
[7] Pelrine, R., Kornbluh, R., Pei, Q. B., and Joseph, J., 2000, "High-Speed Electrically Actuated Elastomers With Strain Greater Than 100%," Science, **287**(5454), pp. 836–839.
[8] Li, T., Keplinger, C., Baumgartner, R., Bauer, S., Yang, W., and Suo, Z., 2013, "Giant Voltage-Induced Deformation in Dielectric Elastomers Near the Verge of Snap-Through Instability," J. Mech. Phys. Solids, **61**(2), pp. 611–628.
[9] Liang, X., and Cai, S., 2018, "New Electromechanical Instability Modes in Dielectric Elastomer Balloons," Int. J. Solids Struct., **132–133**, pp. 96–104.
[10] Wang, F., Yuan, C., Lu, T., and Wang, T. J., 2017, "Anomalous Bulging Behaviors of a Dielectric Elastomer Balloon Under Internal Pressure and Electric Actuation," J. Mech. Phys. Solids, **102**, pp. 1–16.
[11] Mao, G., Huang, X., Diab, M., Li, T., Qu, S., and Yang, W., 2015, "Nucleation and Propagation of Voltage-Driven Wrinkles in an Inflated Dielectric Elastomer Balloon," Soft Matter, **11**(33), pp. 6569–6575.
[12] Godaba, H., Foo, C. C., Zhang, Z. Q., Khoo, B. C., and Zhu, J., 2014, "Giant Voltage-Induced Deformation of a Dielectric Elastomer Under a Constant Pressure," Appl. Phys. Lett., **105**(11), p. 112901.
[13] Wang, H., Cai, S., Carpi, F., and Suo, Z., 2012, "Computational Model of Hydrostatically Coupled Dielectric Elastomer Actuators," ASME J. Appl. Mech., **79**(3), p. 031008.
[14] Suo, Z., 2010, "Theory of Dielectric Elastomers," Acta Mech. Solida Sin., **23**(61), pp. 549–578.
[15] Zhao, X., and Suo, Z., 2007, "Method to Analyze Electromechanical Stability of Dielectric Elastomers," Appl. Phys. Lett., **91**(6), p. 61921.
[16] Lu, T., Cai, S., Wang, H., and Suo, Z., 2013, "Computational Model of Deformable Lenses Actuated by Dielectric Elastomers," J. Appl. Phys., **114**(10), p. 104104.
[17] Moscardo, M., Zhao, X., Suo, Z., and Lapusta, Y., 2008, "On Designing Dielectric Elastomer Actuators," J. Appl. Phys., **104**(9), p. 093503.
[18] Li, J., Liu, L., Liu, Y., and Leng, J., 2019, "Dielectric Elastomer Spring-Roll Bending Actuators: Applications in Soft Robotics and Design," Soft Robot., **6**(1), pp. 69–81.
[19] Zhu, J., Stoyanov, H., Kofod, G., and Suo, Z., 2010, "Large Deformation and Electromechanical Instability of a Dielectric Elastomer Tube Actuator," J. Appl. Phys., **108**(7), p. 74113.
[20] He, T., Cui, L., Chen, C., and Suo, Z., 2010, "Nonlinear Deformation Analysis of a Dielectric Elastomer Membrane–Spring System," Smart Mater. Struct., **19**(8), p. 85017.
[21] Gent, A. N., 1996, "A new Constitutive Relation for Rubber," Rubber Chem. Technol., **69**(1), pp. 59–61.